Non-steady-state photo-EMF interferometer for detection of mechanical oscillations in transparent scattering objects

M.A. BRYUSHININ[1,*], V.V. KULIKOV[1], A.A. PETROV[1], I.A. SOKOLOV[1], R.V. ROMASHKO[2], AND YU.N. KULCHIN[2]

[1] Ioffe Institute, St. Petersburg, Russia
[2] Institute of Automation and Control Processes FEB RAS, Vladivostok, Russia
[*] Corresponding author: mb@mail.ioffe.ru

Compiled February 3, 2020

The operation of adaptive non-steady-state photo-EMF sensor is studied in the interferometric arrangement including the diffuse scattering object – fiber optic plate. The mechanical oscillations of this plate induce the strains and stresses of the medium, which modulate the phase of the propagating light wave across the plate. The resonant frequencies of the mechanical system and the distribution of the phase modulation amplitude across plate's surface are measured. The minimal detectable stress amplitude is estimated.

OCIS codes: (120.1088) Adaptive interferometry; (190.2055) Dynamic gratings.

http://dx.doi.org/10.1364/AO.XX.XXXXXX

1. INTRODUCTION

Holographic interferometry being the most sensitive and versatile method for nondestructive testing of solids, investigations of gas and liquid streams [1], requires solution of an important technical problem – stabilization of the optimal operating point under slowly varying environmental conditions. Along with the active stabilization the methods of dynamic holography are used. There are two main implementations of the adaptive interferometer concept using dynamic space charge gratings: two-wave mixing in photorefractive crystals [2–4] and non-steady-state photo-EMF technique [5, 6]. The former has the better sensitivity and wider frequency range, the latter provides the direct conversion of the optical signals to the electric ones and operation without external voltages. Self-referenced adaptive interferometers using the coherent dipole radiation was also proposed recently [7].

The detection of phase-modulated optical signals using adaptive sensors is usually carried out using the vibrometric scheme, where the light phase incursion is created by the reflection from an oscillating object. Such an additional phase can also appear in the light beam propagating through a stressed transparent material [1]. In our previous work [8] we studied the oscillations of the conventional glass plate using the non-steady-state photo-EMF technique. The effect of the non-steady-state photo-EMF reveals itself as an alternating electric current arising in a semiconductor illuminated by an oscillating interference pattern. The electric current appears due to spatial shifts of the space-charge and photoconductivity distributions in the crystal volume [9]. In this paper we apply this technique to the investigations of the oscillating fiber optic plate (FOP), which is chosen as an example of diffuse scattering medium. The photo-EMF sensor is made of silicon carbide (SiC) crystal, which is a technologically attractive material demonstrating the suitable combination of the signal level and frequency response [10].

2. EXPERIMENTAL SETUP

The detection of mechanical oscillations is performed with the arrangement (Fig. 1) similar to that used in our previous experiments with the transparent glass plate [8]. The laser light with the wavelength of $\lambda = 660$ nm is split into two beams, which then create the interference pattern with the average spatial frequency $K = 2\pi/\Lambda = 8.7\ \mu\text{m}^{-1}$ and intensity $I_0 = 2.2$ W/cm^2 on the detector. The signal beam passes through the fiber optic plate, where it undergoes the diffuse scattering and phase modulation. The scattered light is collected with the lens ($f = 70$ mm) placed at a distance of 150 mm from the plate. The diameter of the collected light spot on the detector's surface is nearly the same as the diameter of the reference beam, i.e. 1.2 mm. The ratio of powers in the object and reference beams is of 6.0 mW/22 mW, the corresponding average contrast of the interference pattern equals $m = 0.82$. The oscillatory stresses in the FOP are created through the lateral cylindrical surface

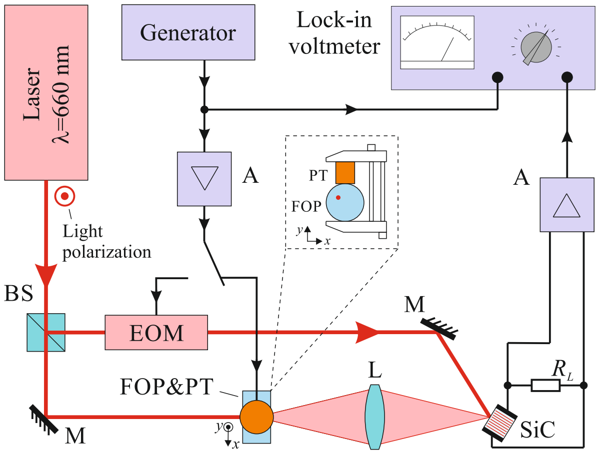

Fig. 1. Interferometric arrangement for the detection of the mechanical oscillations using the non-steady-state photo-EMF sensor.

using the piezoelectric transducer. The clamp with the plate and transducer is settled on the manual stage allowing translation in the plane perpendicular to the laser beam (xy-plane). We use also the electro-optic modulator during the calibration of our SiC detector, it introduces sinusoidal phase modulation with amplitude $\Delta_c = 0.72$ into the reference beam. The photocurrent arising in the detector produces a voltage signal across the load resistor $R_L = 300$ kΩ, which passes through the 20 dB preamplifier with the input impedance of 100 MΩ/0.65 pF, and then it is measured by the lock-in voltmeter. The polarization plane is perpendicular to the plane of incidence to the detector's surface (TE-polarization). The preparation of the SiC sensor was described earlier in Ref. [10]. This is a 6H-SiC crystal preliminarily irradiated by the reactor neutrons with the fluence of 10^{18} cm^{-2}. It has the dimensions of $6.0 \times 1.0 \times 0.38$ mm, the polished front and back surfaces (6.0×1.0 mm) are the (0001) planes. The silver paste electrodes are deposited on the lateral ones.

The fiber optic plate studied in this work is an array of close-packed fibers with the diameter of 5.8 μm (Fig. 2). These fibers are combined into the 450 μm hexagonal clusters, which are merged in their turn forming the whole plate with the diameter of 38 mm and thickness of 9 mm. The front and back surfaces of the FOP are of optical quality, nevertheless the light sustains the diffuse scattering (Fig. 2). One can note six diffraction peaks edging the speckle pattern. The angle between adjacent peaks equals 6.7°, which corresponds to the lattice constant of 5.7 μm.

3. EXPERIMENTAL RESULTS

Since the non-steady-state photo-EMF has not been studied in SiC crystal at the chosen wavelength, we have to start our experiments with the calibration of the detector. First we measured the photoconductivity response to the amplitude-modulated light. This allows us to estimate the resistance and photoconductivity of the sample: 69 GΩ and 2.7×10^{-10} Ω^{-1}m^{-1} for $I_0 = 1.3$ W/cm^2. The phase of the non-steady-state photo-EMF signal corresponds to the electron conductivity of the crystal. The frequency dependence of the signal amplitude, i.e. dependence $J^\omega = J^\omega(\Delta_c, \omega)$, is measured with electro-optic modulator for the certain amplitude of phase modulation Δ_c (Fig. 3). The dependence contains the growth of the signal at low frequencies ω

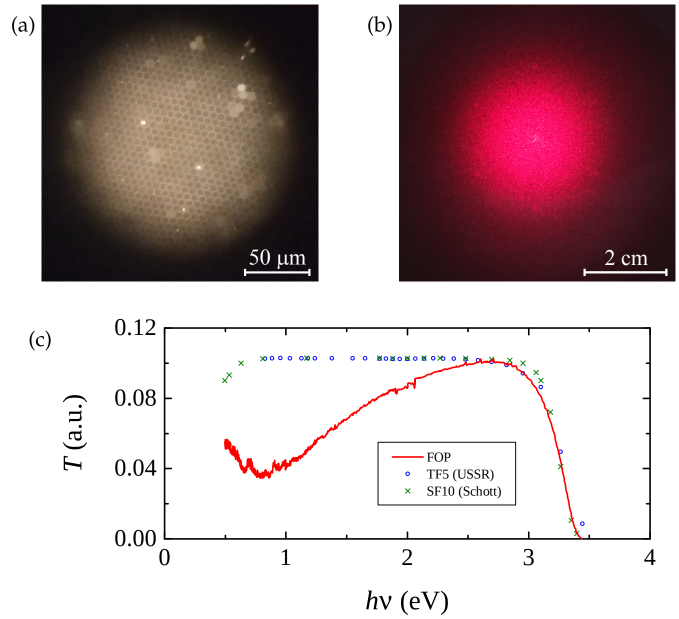

Fig. 2. Microscope image of the fiber optic plate (a), pattern of the scattered light on the lens surface (b), and light transmission spectrum of the investigated FOP (c). The normalized transmission spectra of the heavy flint glasses are also plotted for comparison.

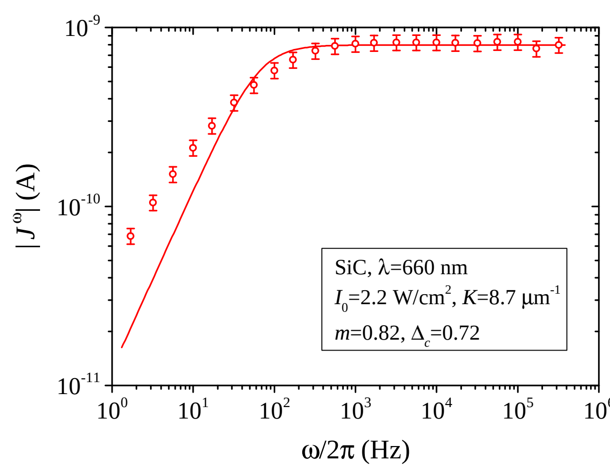

Fig. 3. Frequency dependence of the non-steady-state photo-EMF signal in the SiC adaptive detector.

followed by the frequency independent part. The signal growth at low frequencies is an important manifestation of the adaptivity of space charge formation in photoconductive materials [9, 11]. Both the space charge field grating and the grating of free electrons (photoconductivity grating) follow the interference pattern at low ω. The spatial shift between them keeps nearly equal to $\pi/2$, which results in small value of the average drift component of the current. The grating with larger relaxation time becomes "frozen-in" at higher frequencies, the spatial shifts between the gratings increase, and the current reaches its maximum at the frequency-independent part. There is no decay at high ω, so the space charge grating is recorded in the regime of quasi-stationary photoconductivity ($\omega\tau \ll 1$), and the signal behavior is described by the simple expression [9]:

$$J^\omega = \frac{Sm^2 \, \mathrm{J}_0(\Delta)\, \mathrm{J}_1(\Delta)\sigma_0 E_D}{1+K^2L_D^2}\, \frac{-i\omega/\omega_0}{1+i\omega/\omega_0}, \quad (1)$$

where $\omega_0 = [\tau_M(1+K^2L_D^2)]^{-1}$ is the cut-off frequency separating the growing part and plateau in the frequency dependence, $E_D = (k_B T/e)K$ is the diffusion field, $\tau_M = \epsilon_0\epsilon/\sigma_0$ is the Maxwell relaxation time, L_D is the diffusion length of electrons, J_n is the Bessel function of the first kind of the n-th order, S is the area of the illuminated electrodes, k_B is the Boltzmann constant, T is the temperature, e is the elementary charge, ϵ_0 is the free space permittivity. The spatial frequency is settled close to its optimum value $K = L_D^{-1}$ maximizing the signal amplitude. The cut-off frequency is of 65 Hz for the curve shown in Fig. 3, and it corresponds to the following values of the Maxwell relaxation time and average photoconductivity: $\tau_M = 2.5$ ms, $\sigma_0 = 3.5\times10^{-10}\ \Omega^{-1}\mathrm{cm}^{-1}$. The nonlinear growth of the signal for low frequencies as well as the some discrepancy between values of the signal amplitude and cut-off frequency can be associated with the high light absorption of the crystal [10].

Our interferometer detecting the speckled light operates in a different manner with respect to the scheme dealing with the undistorted beam [8]. The signal at frequencies above 30 kHz is excited as it has been conceived: the signal beam gets phase modulation passing through the stressed media. The dominant contribution at frequencies below 30 kHz appears in the other way: the reference beam reaches the detector surface, the light is partially reflected, it passes the lens and falls onto the back surface of the FOP. Then the light is partially reflected again and returns to the detector, where it interferes with the initial reference light. The phase modulation in this "signal" beam is resulted from the oscillation of the FOP's back surface, which is due to the movements of the sample as a whole and elongation/contraction along z-axis. The light propagating through the FOP is not required in this low-frequency regime at all, it can even reduce the detected signal. The previous experiment [8] with the undistorted signal beam and accordingly comprising no lens in the arrangement was practically free from such a retroreflection, a small angle misalignment did not allow the light return to the detector. The signal at frequencies below 30 kHz can also arise from the in-plane oscillations of the transparent scattering object. The signal appears due to regular shifts of the speckle pattern, the reference beam is not required in this regime [6].

Having characterized the adaptive photodetector we can start investigations of a real oscillating object. The frequency dependence of the non-steady-state photo-EMF signal excited by the FOP oscillations is presented in Fig. 4. Such a dependence is defined by both the "object" and "detector" contributions:

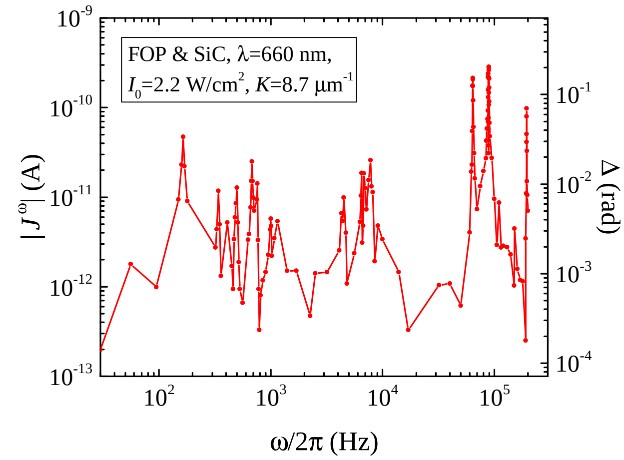

Fig. 4. Frequency dependence of the detected non-steady-state photo-EMF signal and corresponding amplitude of phase modulation produced by the mechanical oscillations of the fiber optic plate.

$J^\omega = J^\omega(\Delta(\omega),\omega)$. As seen from Eq. (1), the amplitude of phase modulation $\Delta(\omega)$ created by the object oscillation is a solution of the following nonlinear equation:

$$\frac{J^\omega(\Delta(\omega),\omega)}{\mathrm{J}_0(\Delta(\omega))\,\mathrm{J}_1(\Delta(\omega))} = \frac{J^\omega(\Delta_c,\omega)}{\mathrm{J}_0(\Delta_c)\,\mathrm{J}_1(\Delta_c)} \quad (2)$$

The mechanical oscillations of the FOP result in the rather small phase modulation amplitudes ($\Delta < 0.22$), and the most of the studied frequency range $0.1-200$ kHz corresponds to the plateau in the frequency dependence of the SiC adaptive detector. This equation can be linearized under the circumstances, and the desired frequency dependence $\Delta(\omega)$ can be calculated just by the multiplication of the measured dependence $J^\omega(\Delta(\omega),\omega)$ by a certain coefficient or by adding another axis in the plot, as it was done in Fig. 4. The resonant behavior of the signal J^ω and calculated amplitude Δ is associated with the mechanical resonances of the system including the FOP, piezoelectric transducer and clamp. The frequency response of the detached piezoelectric transducer was measured in [12] and it has only three maxima in the frequency range 10 Hz – 50 kHz.

Mechanical stresses and deformations distribute non-uniformly in solids, except for the special cases. Besides, the oscillation frequency is high enough, so that the sound wavelength becomes comparable with the dimensions of our FOP. The resulting distribution of the phase modulation amplitude is expected to be non-uniform across the plate surface as well. We have measured this distribution by moving the clamped FOP and transducer in the directions perpendicular to the light beam (Fig. 5). The measurements are performed at two resonant frequencies: 89.54 kHz and 194.28 kHz. The nearly radial symmetry of the former contour plot reminds the one obtained earlier with the transparent glass plate [8]. The map obtained at the latter frequency looks different: it has four maxima, which point out to the excitation of the higher mode of mechanical oscillations. The two of these maxima (at $y \simeq 0$) have the oscillation phase of 0, while the others (at $x \simeq 0$) have the phase of π.

4. DISCUSSION

The procedure, that allows to associate the mechanical stresses with the resulting light phase increments, includes four steps:

(1) the definition of the mechanical stress tensor **œ** in the crystal-physical coordinate system, (2) calculation of dielectric impermeability tensor $\xi_{ij} = \pi_{ijkl}\sigma_{kl}$ in the crystal-physical coordinate system, (3) transformation of tensor ξ to the principal coordinate system which is defined by direction of light propagation, (4) derivation of the refractive indexes $n_{1,2}$ and corresponding components of the electric induction vector $\mathbf{D}$.

There are analytic approaches developed for mechanical oscillations in finite circular rods [13, 14]. They allow calculation of the natural frequencies and corresponding mode shapes for stresses and strains. The solution is usually presented as series with the terms written in the cylindrical coordinates ρ, ϕ, z as follows:

$$\mathfrak{R}_n(\alpha\rho) \begin{Bmatrix} \sin n\phi \\ \cos n\phi \end{Bmatrix} \begin{Bmatrix} \cos \beta z \\ \sin \beta z \end{Bmatrix} \quad \textbf{(3)}$$

The radial function $\mathfrak{R}_n$ can be the Bessel function $\mathrm{J}_n(\alpha\rho)$, its derivative $\mathrm{J}'_n(\alpha\rho)$, functions $\rho^{-1}\mathrm{J}_n(\alpha\rho)$, $\rho^{-1}\mathrm{J}_{n-1}(\alpha\rho)$, $\rho^{-2}\mathrm{J}_n(\alpha\rho)$ and their linear combination. Parameters α, β possesses several values, in particular, α can be the root of equation $\mathrm{J}_n(\alpha R) = 0$, where R is the radius of the cylinder. Our former contour plot evidently corresponds to the excitation of the axisymmetric mode with $n = 0$, and the latter does with $n = 2$. Strictly speaking this analytic approach is valid for isotropic cylinders but not for the structured fiber array. We could simulate stresses numerically [8] but this also requires the numeric values for the tensor of elastic constants.

There is even more significant problem in the mentioned four-step procedure implementation. The light does not propagate as a plane wave. That is why we try to link the measured amplitudes of phase modulation with the mechanical stresses and strains using the results known from the fiber optics.

Let us suppose that each fiber is under the uniform compression, but the value of this pressure P can vary from fiber to fiber. The phase increment arising in the fiber of length L is mostly defined by two factors: the elongation/contraction of the fiber and piezooptic effect [15]:

$$\frac{\Delta}{PL} = -\frac{\beta(1-2\nu)}{E}\left[1 - \frac{n_1^2}{2}(2p_{12} + p_{11})\right], \quad \textbf{(4)}$$

where E is the Young's modulus, ν is the Poisson's ratio, n_1 is the refractive index of the fiber core, β is the propagation constant, p_{11}, p_{12} are the components of the strain-optic tensor. The phase increment resulting from the waveguide mode dispersion effect due to a change in fiber diameter is usually neglected [15]. This is apparently rough approach, but it allows us to estimate the order of magnitude of the stresses. Let us estimate the right hand of Eq. (4) using the material parameters typical for heavy flint glasses (Fig. 2), Schott's SF10, for example [16]: $n_1 = 1.72$, $E = 63.4$ GPa, $\nu = 0.236$, $p_{11} = 0.194$, $p_{12} = 0.234$. The microscope image of the FOP obtained in the transmitted light provides the estimate for the fiber core radius $a = 1.8$ μm. If we assume the cladding refractive index n_2 of 1.5 [17], then the normalized frequency of the fiber equals $V = 14$, and the total number of guided modes equals $V^2/2 = 98$, which explains the appearance of the speckle pattern in the light passing through the FOP. The propagation constant β varies from $(2\pi/\lambda)n_1$ for the low-order modes to $(2\pi/\lambda)n_2$ for higher modes (n_2 is the refractive index of the cladding and it is of 1.5 for FOP). The electromagnetic field of the high-order modes penetrates deeper into cladding and can be partially absorbed with the specially embedded extra-mural absorption fibers [17]. Thus we take β typical

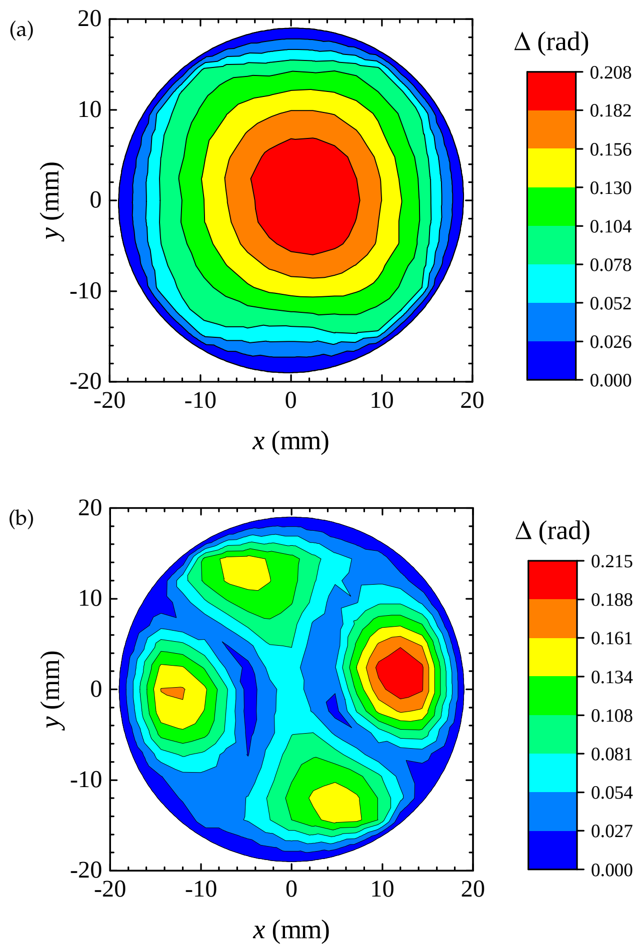

Fig. 5. Distributions of the phase modulation amplitude across the fiber optic plate surface measured at two frequencies: $\omega/2\pi = 89.54$ kHz (a) and 194.28 kHz (b).

for low-order modes, say, $(2\pi/\lambda)1.7$. The substitution of these values into (4) provides $\Delta/PL = -2.8 \times 10^{-6}$ rad·Pa^{-1}m^{-1}. For the observed phase modulation amplitude of $\Delta \simeq 0.2$ and fiber length of $L = 9$ mm (plate thickness) we obtain the estimate for the pressure (stress) amplitude: $P = 7.9$ MPa. The signal-to-noise ratio reaches 600, so the minimal detectable amplitude of mechanical stress is of $\sigma_{min} = 13$ kPa for the detection bandwidth of $\delta f = 1$ Hz. Since a number of assumptions were made this estimate should be considered as very rough. Additional significant errors could arise, if the plate had reflection coatings. Then the fibers would operate as high-quality Fabry-Perot resonators and introduce the higher phase modulation.

The attractive features of the technique such as the high sensitivity, adaptivity and operation with complicated wavefronts are partially compensated by the fact of local point-by-point measurements, while the traditional techniques [1] allow processing of the whole interference pattern. The development of the non-steady-state photo-EMF sensor array could solve this problem, but it is a challenge for the future.

5. CONCLUSION

In conclusion, we have demonstrated the capabilities of the adaptive non-steady-state photo-EMF sensor in detection of mechanical oscillations in diffuse scattering objects. The frequency response and the distribution phase modulation amplitude across fiber optic plate surface were obtained. The technique using this adaptive sensor allows the remote detection of mechanical stress oscillations as small as 13 kPa, which makes it a powerful tool for nondestructive testing of transparent optical materials and elements.

ACKNOWLEDGMENTS

I.S. and Yu.K. acknowledge support grant from the Russian Science Foundation (project no. 19-12-00323).

DISCLOSURES

The authors declare no conflicts of interest.

REFERENCES

1. C. M. Vest, *Holographic interferometry*, Wiley Series in Pure & Applied Optics (John Wiley & Sons, New York, 1979).
2. A. A. Kamshilin, R. V. Romashko, and Y. N. Kulchin, "Adaptive interferometry with photorefractive crystals," *J. Appl. Phys.* **105**, 031101 (2009).
3. S. Di Girolamo, R. V. Romashko, Y. N. Kulchin, and A. A. Kamshilin, "Orthogonal geometry of wave interaction in a photorefractive crystal for linear phase demodulation," *Opt. Commun.* **283**, 128–131 (2010).
4. K. Shcherbin, V. Danylyuk, and M. Klein, "Characteristics of two-wave mixing adaptive interferometer with CdTe:Ge at 1.06 and 1.55 μm and improved temporal adaptability with temperature control," *Appl. Opt.* **52**, 2729–2734 (2013).
5. S. I. Stepanov, I. A. Sokolov, G. S. Trofimov, V. I. Vlad, D. Popa, and I. Apostol, "Measuring vibration amplitudes in the picometer range using moving light gratings in photoconductive GaAs:Cr," *Opt. Lett.* **15**, 1239–1241 (1990).
6. N. A. Korneev and S. I. Stepanov, "Measurement of small lateral vibrations of speckle patterns using a non-steady-state photo-emf in GaAs: Cr," *J. Mod. Opt.* **38**, 2153–2158 (1991).
7. N. Casillas, S. Stepanov, M. Ocegueda, and E. Hernandez, "Utilizing phase memory of a two-level quantum system for adaptive homodyne detection of optical phase modulation," *J. Opt.* **21**, 045201 (2019).
8. M. A. Bryushinin, I. A. Sokolov, and A. M. Balbashov, "Visualization of oscillatory stresses in transparent media using a β-Ga_2O_3 adaptive detector," *Appl. Opt.* **56**, 170–178 (2017).
9. M. P. Petrov, I. A. Sokolov, S. I. Stepanov, and G. S. Trofimov, "Non-steady-state photo-electro-motive force induced by dynamic gratings in partially compensated photoconductors," *J. Appl. Phys.* **68**, 2216–2225 (1990).
10. M. A. Bryushinin, V. V. Kulikov, E. V. Mokrushina, E. N. Mokhov, A. A. Petrov, and I. A. Sokolov, "Non-steady-state photoelectromotive force in SiC crystals irradiated by reactor neutrons," *Phys. Solid State* **56**, 1939–1946 (2014).
11. M. P. Petrov, S. I. Stepanov, and A. V. Khomenko, *Photorefractive crystals in coherent optical systems*, vol. 59 of *Springer Series in Optical Sciences* (Springer-Verlag, Berlin Heidelberg, 1991).
12. I. A. Sokolov, P. Hess, M. A. Bryushinin, V. V. Kulikov, S. H. Khan, and K. T. V. Grattan, "Adaptive photodetectors using the effect of the non-steady-state photoelectromotive force for vibration measurements," in *Interferometry in speckle light: Theory and applications,* P. Jacquot and J.-M. Fournier, eds. (Springer, Berlin-Heidelberg, 2000), pp. 187–194.
13. S. N. Rasband, "Resonant vibrations of free cylinders and disks," *J. Acoust. Soc. Am.* **57**, 899–905 (1975).
14. J. R. Hutchinson, "Vibrations of solid cylinders," *J. Appl. Mech.* **47**, 901–907 (1980).
15. G. B. Hocker, "Fiber-optic sensing of pressure and temperature," *Appl. Opt.* **18**, 1445–1448 (1979).
16. O. Lindig, *Spannungsdoppelbrechung in Gläsern*, vol. II/8 of *in Optical Constants, Landolt-Börnstein* (Springer, Berlin, Heidelberg, 1962).
17. SCHOTT North America, Inc., "An introduction to fiber optic imaging," Southbridge, MA, USA.